

The compressive response of the filled Kelvin foam

J. Carlsson, V S Deshpande and N A Fleck

Cambridge University Engineering Dept., Cambridge, CB2 1PZ, UK

28 April 2023

Abstract

Periodic unit-cell solutions are obtained for the finite-strain, elasto-plastic response of a filled closed-cell Kelvin foam in uniaxial compression. The closed-cell Kelvin foam has edges of equal length, and attention is focussed on the regular Kelvin foam with faces comprising regular hexagons and squares. The elongated Kelvin foam is also studied: its faces comprise elongated hexagons and quadrilaterals. Both the cell walls and core of the Kelvin foam are treated as elastic, ideally plastic von Mises solids. In the first part of the study, the core modulus and strength are sufficiently small for the core to behave as an inviscid, incompressible fluid. Filling of the closed-cell Kelvin foam, in regular or elongated form, with an inviscid, incompressible core elevates its yield strength slightly and stabilises the post-yield response against softening. In the second part of the study, the macroscopic modulus and strength of a filled closed-cell foam are determined as a function of core modulus and deviatoric strength. The deformation mode of the cell edges switches from a bending mode to an affine stretching mode when the core is sufficiently stiff and strong; an analytical model is derived for affine deformation of cell walls and core. Finally, the response of a finite specimen containing an edge imperfection is in good agreement with the periodic, unit cell response of the filled Kelvin foam.

Keywords: Kelvin foam, multi-phase cellular solids, affine deformation, shear localisation

1. Introduction

The recent emergence of additive manufacture has led to increased interest in the design and application of cellular solids with a periodic three-dimensional (3D) lattice architecture. Expansion of material property space is possible by the invention of interpenetrating multi-lattices where the voids in the lattice are filled by either another solid or a liquid, in order to enhance macroscopic stiffness and strength. A literature is emerging on two interpenetrating open-cell lattices with interconnected porosity as a third phase, see for example White et al. (2021); a representative example is the face-centred cubic octet truss inter-penetrating the rhombic dodecahedron. Compressive response of two-dimensional (2D) and 3D lattice materials with a compressible foam core has been explored by Cartié and Fleck (2003), Yan et al. (2013), and the recent review by Han et al. (2017). The foam core can act to stabilise the lattice against elastic or plastic buckling and change the buckling mode. The structural benefit achieved by filling the air gaps of a lattice-cored sandwich panel with a ceramic polymeric foam has also been explored, see Han et al (2017).

Filled hexagonal honeycombs have been studied analytically and numerically by Tankasala et al. (2021) and Carlsson et al. (2022). These studies reveal that the filling of a honeycomb by an inviscid, incompressible fluid (or solid) can replace bending-dominated deformation modes by stretching-dominated modes of significantly higher strength. The authors have not been able to find any analyses of 3D closed-cell lattices filled by an incompressible medium, hence the need for the present study.

Closed-cell foams with solid cell walls are commonly manufactured from the molten state by the solidification of a liquid foam. As foaming proceeds in the liquid state, the cell size increases and the cell morphology evolves in order to minimise surface energy. Consequently, the microstructure tends towards a minimum surface structure, such as the Kelvin foam (Kelvin, 1887) or the Weaire–Phelan structure (Weaire and Phelan, 1994; Weaire and Hutzler 2001). To date, the Weaire–Phelan structure has the smallest known surface area per cell, 0.3% less than that of the Kelvin structure, and comprises a combination of irregular dodecahedra with pentagonal faces, and tetrakaidecadra made from two hexagonal and twelve pentagonal faces. The Kelvin structure is simpler; it is a tetrakaidecadron made from 6 quadrilaterals and 8 hexagons, as shown in Fig. 1(a); in its regular form, all edges are of the same length and the quadrilaterals become squares. The Kelvin structure is a common idealisation for open-cell foams, and is also an excellent representation of a closed-cell foam upon adding faces

(hexagons and squares). The present study explores the effect of filling of a closed-cell Kelvin foam upon its macroscopic compressive response.

We shall focus our attention on a closed-cell Kelvin foam, with side length ℓ of all edges. The shape of the Kelvin foam is defined by the included angle 2ω of the quadrilateral faces as defined in Fig. 1(a); for the choice $\omega = \pi/4$ the quadrilateral faces are squares and the Kelvin foam is termed regular. When ω exceeds $\pi/4$, the Kelvin foam is elongated. The dependence of volume V of unit cell upon the internal angle of face ω for the 3D closed-cell Kelvin foam is qualitatively similar to that for the two-dimensional (2D) hexagonal honeycomb of Fig. 1(b): the volume of the unit cell depends upon angle ω , with a maximum value at an intermediate value of $\omega = 45^\circ$ for the Kelvin foam and $\omega = 30^\circ$ for the hexagonal honeycomb, where ω for the honeycomb is defined in Fig. 1(b). The dependence of V upon ω is expressed in analytical form by

$$\frac{V}{\ell^2} = 2(1 + \sin \omega) \cos \omega, \quad (1.1)$$

for the hexagonal honeycomb (Tankasala et al., 2021), and

$$\frac{V}{\ell^3} = 2 \sin \omega (\sqrt{2} + 2 \sin \omega)^2, \quad (1.2)$$

for the closed-cell Kelvin foam (see Sullivan et al. (2009), for example)). Both relations are plotted in Fig. 1(c). The relative density $\bar{\rho}$ of the hexagonal honeycomb is directly related to V by

$$\bar{\rho} = \frac{3t\ell}{V} = \frac{3t}{2\ell} (1 + \sin \omega)^{-1} \sec \omega, \quad (1.3)$$

where t is the cell wall thickness, while for the Kelvin unit cell, with edges of circular cross-section of diameter d and no faces, we have

$$\bar{\rho} = \frac{3\pi d^2 \ell}{V} = 3\pi \left(\frac{d}{\ell}\right)^2 (1 + \sqrt{2} \sin \omega)^{-2} \csc \omega. \quad (1.4)$$

Tankasala et al. (2021) and Carlsson et al. (2022) showed that the compressive response of the filled hexagonal honeycomb is highly sensitive to the value of ω , and we shall determine whether this finding extends to that of the filled Kelvin foam.

1.1 The compressive strength of a 2D hexagonal lattice filled by an inviscid, incompressible solid

Carlsson et al. (2022) recently found that filling a hexagonal honeycomb by an incompressible solid has a dramatic effect upon its in-plane compressive response. A major aim of the present study is to determine whether this also holds for the closed-cell Kelvin foam. First, we summarise the main relevant findings of Carlsson et al. (2022). They assumed that the cell walls and core both comprise elastic, ideally plastic von Mises solids, such that the uniaxial strength of the core material is much less than that of the cell walls. Consequently, the core material behaves as an inviscid, incompressible fluid, or equivalently as an incompressible solid of negligible deviatoric modulus and strength. The honeycomb has sides of equal length, and its inclined cell walls subtend an angle ω with respect to the transverse direction that can deviate from the usual value of 30° which is characteristic of a regular honeycomb, see Fig. 1(b). Two responses of the core material were assumed: the fully bonded, ‘non-cavitating core’ (in the presence of a sufficiently high macroscopic pressure) and a ‘cavitating core’ that can cavitate or debond freely from the cell walls.

Carlsson et al. (2022) obtained finite strain, finite element numerical solutions for both empty and filled hexagonal honeycombs, thereby building upon the small strain analysis of Tankasala et al. (2021). When the cell walls are inclined at $\omega = 30^\circ$ the initial, small strain compressive response of the *empty* honeycomb involves the formation of inextensional plastic hinges in the cell walls. Consequently, the macroscopic yield strength σ_Y scales with the square of the relative density $\bar{\rho}$. This collapse occurs at constant volume and so the addition of an incompressible core of vanishing deviatoric strength has no effect upon the initial collapse response. As macroscopic compressive straining proceeds, however, the empty honeycomb loses volume and crush bands form in a softening manner. The addition of an incompressible core precludes this post-yield mode of inextensional plastic bending of cell walls at finite strain of the honeycomb, and extensional plastic hinges now develop in the cell walls, along with rapid strain hardening in the macroscopic compressive response.

We emphasise that the regular honeycomb with cell walls inclined at $\omega = 30^\circ$ is an extremal structure such that the volume of the unit cell, with sides of equal length, is a maximum for this choice of ω , recall Fig. 1(c). This has a major implication for the compressive response at $\omega > 30^\circ$. For example, consider an elongated honeycomb such that its initial configuration is $\omega = 40^\circ$. Then, macroscopic compression of the empty elongated honeycomb leads to dilatation of

the unit cell by plastic hinge formation, and the macroscopic yield strength σ_Y again scales as $\bar{\rho}^2$. The presence of a cavitating core does not change this initial response. In contrast, dilatation is prevented by the presence of a non-cavitating core, and the initial yield response requires stretching of the cell walls; consequently, the compressive yield strength scales linearly with $\bar{\rho}$. Carlsson et al (2022) report that the macroscopic yield strength σ_Y is given by

$$\frac{\sigma_Y}{\bar{\rho}\sigma_0} = \frac{2}{\sqrt{3}} \frac{\sin \omega - \cos 2\omega}{3 \sin \omega}, \quad (1.5)$$

where σ_0 is the yield strength of the cell walls. The prediction (1.5) for $\omega = 40^\circ$ is denoted by a horizontal line in Fig. 2(a). This initial deformation mode is soon followed by a strongly softening shear mode of deformation that does not require cell wall stretching. Carlsson et al (2022) derived an analytical formula for this softening mode such that the macroscopic stress σ^∞ versus macroscopic plastic strain ε_p^∞ reads

$$\frac{-\sigma^\infty}{\bar{\rho}^2\sigma_0} = 0.138 \left(-\varepsilon_p^\infty\right)^{-\frac{1}{2}}, \quad (1.6)$$

for the case $\omega = 40^\circ$, as plotted in Fig. 2(a). Carlsson et al (2022) also performed finite element simulations of finite specimens containing an edge defect and found that the dominant collapse mode is by the formation of inclined shear bands. This mode of shear localisation resembles fibre kinking in a long fibre composite, see for example, Fleck (1997). In contrast, shear localisation in metallic alloys is associated with the nucleation, growth and coalescence of voids. Tvergaard has pioneered our understanding of ductile fracture and has given the numerical underpinning to explain a wide range of observed phenomena ranging from tensile failure of a metallic sheet by shear bands to crack advance by void growth, see for example Tvergaard (1982) and Tvergaard and Hutchinson (1992).

In summary, the addition of an inviscid, incompressible core to a hexagonal honeycomb has no effect upon the compressive yield strength for the regular geometry of $\omega = 30^\circ$, but has a major impact for an elongated hexagonal honeycomb of $\omega = 40^\circ$ when the core is prevented from cavitating, for example by the imposition of a large external pressure to maintain isochoric deformation. To emphasise this, the compressive strengths of the empty and filled honeycomb of $\omega = 40^\circ$ are plotted as a function of relative density in Fig. 2(b). The presence of a non-cavitating core changes the dependence of σ_Y upon $\bar{\rho}$ from quadratic to linear, resulting in a major difference in strength in the practical range of $\bar{\rho} \ll 1$.

The nodal connectivity of the empty, open-cell Kelvin foam is 4; this is less than the required nodal connectivity of 6 which is required to give the possibility of a stiff, stretching-governed response (Deshpande et al., 2001). Consequently, the empty open-cell Kelvin foam deforms plastically by the formation of inextensional plastic hinges. But the question remains: does the presence of an incompressible core have a major effect upon the compressive strength? We shall address this question in the main body of the paper.

1.2 Compressive response of an empty Kelvin foam

A limited number of studies exist on the compressive response of empty open-cell and empty closed-cell Kelvin foams, but the authors were unable to find any studies that explored the effect of filling of a closed-cell foam by a second phase. There is a limited literature on the mechanics of transverse crushing of a filled honeycomb. D’Mello and Waas (2013) explored the in-plane compressive response of a circular cell, hexagonally packed, thin-wall polycarbonate honeycomb in two states: empty and filled with a polymethylsiloxane (PDMS) elastomer. Both the mode of crushing and the crush strength are sensitive to the presence of the PDMS core. In the empty state, the honeycomb undergoes progressive row-wise collapse. In contrast, in the filled state, the response is stable with no evidence of localisation by crush band formation. The micromechanical basis for the properties of liquid-filled cells in adipose tissue is a related topic, see for example Comley and Fleck (2010). We proceed to summarise the main results from the literature on the compressive properties of an empty open-cell and an empty closed-cell Kelvin foam.

First, it is necessary to review the role of Plateau Borders in the mechanical response of a Kelvin foam. Commonly, manufacture from the molten state leads to an accumulation of solidified material at the nodes of an open-cell foam (and at the edges of a closed cell foam). This is illustrated in Fig. 3(d) for the case of a Kelvin foam. Following Gibson and Ashby (1997), write ϕ as the fraction of cell wall material that resides in the cell edges, such that $\phi > 0$ implies the existence of Plateau Borders. Gibson and Ashby (1997) have developed simple scaling relations for the contribution to macroscopic stiffness and strength from the cell edges and the cell faces in a closed-cell Kelvin foam. At the simplest level, the nodal connectivity of the cell edges is sufficiently small that the cell edges bend and contribute to the macroscopic modulus in a manner that scales with $\bar{\rho}^2$, and to the macroscopic strength in a manner that

scales with $\bar{\rho}^{3/2}$. If cell faces are present (the closed-cell case), then the cell faces stretch and contribute additionally to the macroscopic modulus and strength in a manner that scales with $\bar{\rho}$.

Open-cell Kelvin foam

Open-cell Kelvin foams are commonly used to represent the microstructure of polymeric, metallic and ceramic open-cell foams (Gibson and Ashby, 1997; Ashby et al., 2000). The macroscopic elastic properties of the open-cell regular Kelvin foam have been determined in a comprehensive manner by Warren and Kraynik (1997) and by Zhu et al (1997a,1997b). Sullivan et al. (2008, 2009) extended this analysis to the case of an elongated Kelvin foam. Jang et al (2009, 2010) explored the macroscopic stiffness and compressive strength of a regular open-cell Kelvin foam ($\omega = 45^\circ$); they considered both a unit cell and a finite specimen, and found that both representations give almost identical predictions of modulus and strength. Mild softening is observed in the periodic unit cell due to a finite change in geometry, whereas finite specimens of Kelvin cells give rise to inclined crush bands that extend across the width of the specimen, and then broaden. In contrast, a finite specimen made from irregular Kelvin cells give rise to a random distribution of short-length, isolated crush bands; the prediction for the imperfect foam is much closer to that observed in a foam made from the aluminium alloy 6101-T6. Despite these differences in compressive response beyond peak load, it is evident from the studies of Jang et al. (2009, 2010) that the unit cell representation is adequate for the initial elastic-plastic response.

Closed-cell Kelvin foam

Closed-cell foams are commonly used as the core of sandwich panels and for thermal insulation. For example, rigid closed-cell polyurethane foam was used as insulation on the US space shuttle external tank to limit propellant boil off, and to prevent ice formation. The integrity of the foam was critical: the cause of the space shuttle Columbia disaster on 1 February 2003 was traced to the failure of this foam insulation during launch, leading to damage to the spacecraft's heat shield¹.

¹ <https://history.nasa.gov/columbia/CAIB.html>

Simone and Gibson (1998) explored the effect of Plateau Borders on the elastic and plastic properties of a closed-cell Kelvin foam. They performed a finite element analysis to calibrate analytical expressions for the macroscopic modulus and yield strength in terms of relative density. Compression of closed-cell Kelvin foams to large strain leads to the localisation of crush bands (Chen et al., 2018) in a similar manner to that of open-cell foams. Yield is followed by softening and then the emergence of crush bands during which the foam deforms at near-constant macroscopic stress until, at a strain on the order of unity, significant densification occurs and the stress required to continue deformation increases rapidly. At a sufficiently low value of relative density, elastic buckling intervenes for both open and closed cell foams, see for example Gibson and Ashby (1997) and Deshpande and Fleck (2001).

2 Finite element analysis of an empty Kelvin foam, and a Kelvin foam filled with an incompressible core of negligible shear modulus and strength

2.1 Finite element formulation of the closed-cell Kelvin foam

Finite element simulations are performed on both *empty* and *filled* closed-cell Kelvin foams. Periodic cell calculations were performed using ABAQUS/Standard² with the unit cell comprising two Kelvin polyhedra, see Fig. 3. The general case of an elongated Kelvin foam comprises six rhombuses and eight irregular hexagons, recall Fig. 1(a). The two Kelvin polyhedra fill a cuboidal representative volume element of dimension $D \times D \times H$ where $D = \sqrt{2}\ell (1 + \sqrt{2}\cos \omega)$ and $H = 4\ell \sin \omega$, as explained by Sullivan et al. (2009), and as sketched in Fig. 3. For the elongated Kelvin foam, all edge lengths are of length ℓ and the internal angles of each rhombus are chosen to be $\omega = 55^\circ$; for the regular Kelvin cell, each rhombus becomes a square such that $\omega = 45^\circ$ and each hexagon becomes regular. A Cartesian reference frame (x_1, x_2, x_3) is introduced in Fig. 3, with x_3 aligned with the loading direction.

The cell walls are idealised as an elastic-perfectly plastic von Mises solid of Young's modulus E_0 , Poisson ratio $\nu_0 = 0.3$, and yield strength³ $\sigma_0 = 10^{-3}E_0$. The cell faces are

² ABAQUS/Standard version 2018. Dassault Systèmes Simulia Corp., Providence, RI, USA.

³ The yield strength of steels can be as low as 400 MPa, with minor strain hardening. Such steels have a ratio of yield strength to modulus of 0.002. Also, the choice of a low yield strain reduces the significance of elastic buckling in the calculations.

modelled by plates of thickness t and the edges are treated as beams of circular cross-section and diameter d , see Fig. 3(e). Both the shell thickness t and beam diameter d are varied, with the edge length ℓ held fixed. The relative density of the lattice is denoted $\bar{\rho}$. The fraction of cell wall material that resides in the edges of the unit cell is denoted by ϕ such that $0 \leq \phi \leq 1$. Note that a large value of ϕ , for example $\phi = 0.95$, implies a large Plateau Border while the choice $\phi = 1$ denotes an open-cell Kelvin foam.

The faces of the Kelvin foam were modelled as plate elements (S4R and S3R shell elements in ABAQUS notation). These faces meet along their edges to define the Kelvin foam in the case of vanishing Plateau Borders, $\phi = 0$. When pronounced Plateau Borders were present ($\phi = 0.95$) the faces were again treated as shell elements, whereas the edges were beam elements of circular cross-section (element type B31 in ABAQUS notation). The beam elements share nodes with the underlying shell. Previous studies on empty closed-cell Kelvin foams have shown good agreement between the predictions using shell and solid element models (Simone and Gibson, 1998; Chen et al., 2018). An element length of $\ell/10$, where ℓ is the side length of the sides of the polyhedron, gives sufficient accuracy of prediction for both stiffness and strength. The resulting model typically contained 2×10^4 degrees of freedom.

The core of the filled Kelvin foam is modelled as an almost incompressible elastic-perfectly plastic von Mises solid of shear strength much less than that of the cell wall material. This solid has a Young's modulus of $E_c = 3 \times 10^{-4} E_0$, yield strength $\sigma_c = 10^{-3} E_c$ and Poisson's ratio $\nu_c = 0.4999$. The core is meshed using first order, linear pressure tetrahedral continuum elements (C3D4H) of element side length on the order of $\ell/10$. The resulting model typically has 10^5 degrees of freedom. The core is tied to the cell walls so that cavitation is prevented.

Periodic boundary conditions were imposed on all sides of the cuboidal unit cell of Fig. 3(b), and the macroscopic transverse stresses vanish (natural boundary conditions). Uniaxial compression is generated by imposing a relative axial displacement between nodes on the top face and identically positioned nodes on the bottom face of the unit cell. The rotational degrees of freedom are equal for corresponding nodes on opposing sides of the periodic unit cell.

2.2 Collapse response of the closed-cell Kelvin foam: empty versus filled cores

The macroscopic nominal stress σ^∞ versus nominal strain ε^∞ response of the empty and filled Kelvin foams are given in Fig. 4(a) for the regular geometry of $\omega = 45^\circ$ and in Fig.

4(b) for the elongated Kelvin foam of $\omega = 55^\circ$. Note that the aspect ratio of face sheet thickness t to edge length ℓ of the Kelvin foam absent the Plateau Borders (that is $\phi = 0$) is held fixed at $t/\ell = 0.025$ for both choices of ω , giving $\bar{\rho} = 0.03$ for the regular foam and $\bar{\rho} = 0.032$ for the elongated foam. It is instructive to compare the deformation modes of the regular Kelvin foam ($\omega = 45^\circ$) at two selected values of macroscopic strain, for each type of foam: empty versus filled, and for $\phi = 0$ and 0.95. Accordingly, the deformed Kelvin foam at a macroscopic strain of $|\varepsilon^\infty| = 0.006$ and 0.04 are shown:

- (i) in Fig. 5 as states A and B for the empty foam and $\phi = 0$,
- (ii) in Fig. 6 as states C and D for the empty foam and $\phi = 0.95$,
- (iii) in Fig. 7 as states E and F for the filled foam and $\phi = 0$, and
- (iv) in Fig. 8 as states G and H for the filled foam and $\phi = 0.95$.

Deformed meshes, along with contours of von Mises plastic strain are shown for the face sheets in Figs. 5 to 8, and contours of von Mises stress are included in Figs. 6 and 8 for the case where Plateau Borders exist ($\phi = 0.95$).

First consider the reference case of an empty, closed-cell regular Kelvin foam for $\phi = 0$ and 0.95, see Fig. 4(a). The faces stretch and the edges bend, thus the modulus and yield strength of the Kelvin foam are greater for $\phi = 0$ than for $\phi = 0.95$ (where pronounced Plateau Borders are present). Post yield, wrinkling of the hexagonal faces of the $\phi = 0$ foam accompanies macroscopic compressive straining and leads to macroscopic softening, as shown in the deformed configurations of Fig. 5. The distribution of von Mises strain within the cell walls is included in the deformed meshes, and reveals the nature of the strain localisation. In contrast, for the case of $\phi = 0.95$, the macroscopic load is carried mainly by the cell edges; plastic hinges develop in the cell edges, see Fig. 6 and mild geometric softening occurs, as shown in Fig. 4(a). Face sheet wrinkling occurs in both the square and hexagonal faces, with the largest values of von Mises strain in the square faces. The sum of transverse nominal strains in the x_1 and x_2 directions at a macroscopic nominal strain of $\varepsilon^\infty = -0.04$ is a measure of the degree of shrinkage of the empty unit cell: a sum equal to 0.041 denotes an incompressible response. This sum equals 0.023 for $\phi = 0$ (state B) and increases somewhat to 0.038 for $\phi = 0.95$ (state D). Thus, both empty foams lose volume in the empty state, and we anticipate that the addition of an incompressible core will stiffen the response, particularly for the case $\phi = 0$. We proceed to explore the case of a filled closed-cell regular Kelvin foam for $\phi = 0$ and 0.95.

Filling of the foam slightly elevates the yield strength and stabilises the post-yield collapse to an almost ideally plastic response for $\phi = 0$ and a hardening response for $\phi = 0.95$, see Fig. 4(a). A similar behaviour has been noted by Carlsson et al (2022) for the regular honeycomb ($\omega = 30^\circ$): filling of the honeycomb by an incompressible core does not elevate the yield strength but does eliminate post-yield softening and crush banding. Filling of the Kelvin foam also has a significant effect upon the deformation mode, compare Fig. 7 with Fig. 5 for the case $\phi = 0$, and compare Fig. 8 with Fig. 6 for the case $\phi = 0.95$. In particular, filling of the Kelvin foam reduces the degree of wrinkling of the hexagonal and square faces at a macroscopic compressive strain of 0.04 for the case $\phi = 0$ and eliminates wrinkling of the faces for the case $\phi = 0.95$. Hydrostatic pressure developed in the core of the Kelvin foam for both filled cases ($\phi = 0, 0.95$) and consequently the Plateau Borders develop axial tensile stress for $\phi = 0.95$.

The compressive response of the elongated Kelvin foam is contrasted with that of the regular Kelvin foam, see Figs. 4(a) and (b). In broad terms, filling of the core of the elongated Kelvin foam leads to a small elevation in yield strength for $\phi = 0$ and to a moderate elevation for $\phi = 0.95$; however, there is not a dramatic qualitative change in behaviour upon comparing the elongated Kelvin foam of Fig. 4(b) to the regular Kelvin foam of Fig. 4(a). The presence of the incompressible core stabilises the post-yield response of the elongated Kelvin foam of geometry $\phi = 0$ such that macroscopic softening does not immediately follow yield. Now consider in more detail the elongated Kelvin foam with Plateau Borders present, such that $\phi = 0.95$. Recall from Fig. 1 that axial compression of the open-cell Kelvin foam will reduce the value of ω from the initial value of 55° , and consequently the volume of the unit cell increases. This may lead to cavitation of the core, such that it separates from faces. In our simulations we enforce that such cavitation does not occur, and this is the practical case in the presence of a large superposed pressure at the macroscopic level. Consequently, the core enforces an isochoric collapse mode in contrast to dilation of the empty elongated Kelvin foam. This switch in collapse mode elevates the strength of the foam somewhat, as shown in Fig. 4(b). However, this elevation in strength is much less than that observed upon filling of a hexagonal honeycomb of side inclination $\omega = 40^\circ$, recall Fig. 2. Also, the filled honeycomb has a strongly softening post-yield response, see Fig. 2(a).

A check is made in Appendix A on the relevance of periodic unit cell calculations to the collapse response of a finite specimen with an edge defect in the form of a missing Kelvin

cell. In broad terms, the above findings for a periodic unit cell are preserved for the filled Kelvin foam of geometry $\omega = 45^\circ$ and 55° , and $\phi = 0$ and 0.95 , see Fig. A.1. In particular, there is no evidence of shear band formation, in contrast to the 2D case of a filled hexagonal honeycomb in elongated form ($\omega = 40^\circ$), as explained in the Introduction.

2.3 Sensitivity of modulus and yield strength of filled Kelvin foam to relative density

Recall from the Introduction that filling of a regular honeycomb by a weak incompressible core leads to a negligible increase in macroscopic modulus and yield strength for the regular honeycomb, $\omega = 30^\circ$. In contrast, the modulus and yield strength of the elongated honeycomb ($\omega = 40^\circ$) increase dramatically when an incompressible core has been added. This elevation in strength is a consequence of the switch in deformation mode of the elongated honeycomb from bending-dominated to stretching-dominated due to imposition of a volumetric constraint. It is evident from the previous section that there is no such dramatic switch in behaviour when the 3D elongated Kelvin foam is filled by an incompressible core.

The effect of filling a closed cell Kelvin foam by an inviscid, incompressible solid (or fluid) upon its macroscopic modulus E and strength σ_Y is given in Fig. 9 for a relative density in the range 0 to 0.05. Plots are given for both a regular Kelvin foam ($\omega = 45^\circ$) and an elongated Kelvin foam ($\omega = 55^\circ$), and for vanishing Plateau Borders $\phi = 0$ and dominant Plateau Borders $\phi = 0.95$. The core modulus and strength is $E_c/E_0 = \sigma_c/\sigma_0 = 0.0003$ and the Poisson's ratios are $\nu_o = 0.3$ for the solid and $\nu_c = 0.4999$ for the core. The same broad conclusions hold as those stated for the specific choice of relative density $\bar{\rho} = 0.032$ in the previous section, and are summarised as follows.

(i) The presence of an inviscid, incompressible core has only a minor effect upon the macroscopic modulus and yield strength of the regular and elongated Kelvin foam.

(ii) The collapse strength of the empty and filled Kelvin foam (both regular and elongated) is dictated by plastic collapse, except at very low relative density when elastic buckling intervenes. The following estimates of the transition value of relative density to result in elastic buckling is now summarised.

Recall that the elastic buckling strength σ_b of an open-cell foam ($\phi = 1$) is

$$\sigma_b = 0.05\bar{\rho}^2 E_0 \quad (2.1)$$

and the macroscopic yield strength σ_Y is

$$\sigma_Y = 0.3\bar{\rho}^{3/2}\sigma_0, \quad (2.2)$$

as given by Equations (5.18a) and (5.27a), respectively, of Gibson and Ashby (1997). The transition value of relative density at which macroscopic strength switches from elastic buckling to plastic yield is obtained by equating the above two expressions for strength, giving $\bar{\rho} = 36(\sigma_0/E_0)^2$. In our study we take $\sigma_0/E_0 = 10^{-3}$ and so yielding dominates in the practical regime of $\bar{\rho} > 3.6 \times 10^{-5}$.

Following Gibson and Ashby (1997), the transition value of $\bar{\rho}$ in the absence of Plateau Borders, $\phi = 0$, is obtained by equating (2.1) to the expression

$$\sigma_Y = 0.45\bar{\rho}\sigma_0, \quad (2.3)$$

taken from Simone and Gibson (1998) to give $\bar{\rho} = 9\sigma_0/E_0 = 0.9\%$ for our choice of $\sigma_0/E_0 = 10^{-3}$. Consequently, the response for $\phi = 0$ is dominated by elastic buckling at $\bar{\rho} < 1\%$.

3. Effect of filling of a regular Kelvin foam by an incompressible core of finite modulus and strength

So far our study has considered an incompressible core of negligible shear modulus and shear strength. What is the effect of a finite shear modulus and strength upon the macroscopic properties of the closed-cell Kelvin foam? In order to assess this, we limit attention to the practical case of a regular Kelvin foam with pronounced Plateau Borders ($\phi = 0.95$). As the shear modulus and deviatoric strength of the core increase, the deformation mode of the Kelvin foam progressively changes to become affine, such that the axial stretch of the struts are dictated by deformation of the core. Continue to use the notation of E_0 , E_c and E for Young's modulus of the cell wall, core and filled Kelvin foam, respectively. Likewise, σ_0 , σ_c and σ_Y denote the yield strength of the cell walls, core and filled Kelvin foam, respectively. Then, define the macroscopic modulus ΔE and compressive yield strength $\Delta\sigma_Y$ of the filled Kelvin foam, *relative* to that of the core, as

$$\Delta E \equiv E - E_c \quad \text{and} \quad \Delta \sigma_Y \equiv \sigma_Y - \sigma_c \quad (3.1)$$

Plots of $\Delta E/E_0$ and $\Delta \sigma_Y/\sigma_0$ versus $\bar{\rho}$ are given in Fig. 10 for selected values of E_c/E_0 and σ_c/σ_0 . The core is almost incompressible by taking $\nu_c = 0.4999$. For sufficiently small values of $E_c/E_0 < 0.01$ and $\sigma_c/\sigma_0 < 0.01$ the core behaves as an almost incompressible solid of negligible shear modulus and the macroscopic composite modulus and strength only slightly exceed those for an empty foam.

As E_c/E_0 and σ_c/σ_0 increase, the filled foam adopts a deformation mode that increasingly conforms to affine deformation of the core and Kelvin foam: the pointwise strain state in the core is uniform and is given by $\varepsilon_{33} = \varepsilon_{33}^\infty$, along with $\varepsilon_{11} = \varepsilon_{22} = -(1/2)\varepsilon_{33}^\infty$. In this regime, the foam behaves as a mesh reinforcement, and the Kelvin foam deforms in the manner of the core. Specifically, the vertices of the foam displace with the core and the cell edges and faces are thereby stretched as struts and plates. An additional simplification is made for the case of large Plateau Borders, $\phi = 0.95$. We shall assume that the faces deform in a strut-like manner and thereby assume that, for a given value of relative density, the Kelvin foam of $\phi = 0.95$ deforms in the same manner as $\phi = 1$.

The finite element simulations idealise the foam by an assembly of beams and plates of vanishing physical thickness and so the volume fraction of the core in the finite element mesh is unity instead of $(1 - \bar{\rho})$. Thus, an affine prediction for the composite response takes the form of (3.1), with $\Delta E = \alpha_1 \bar{\rho} E_0$ and $\Delta \sigma_Y = \alpha_2 \bar{\rho} \sigma_0$. Here the constants α_1 and α_2 arise from the fact that the foam edges (and faces) are stretched in a one-dimensional manner between their end vertices. An affine calculation is now reported to show that $\alpha_1 = 1/8$ and $\alpha_2 = 1/6$.

3.1 Upper bound predictions

A straightforward upper bound is now obtained for the contribution by the Kelvin foam to the macroscopic response. We assume that the cell edges of the Kelvin foam are stretched in a compatible manner with the affine displacement imposed on the vertices by affine deformation of the core.

Consider a single, regular Kelvin cell ($\omega = 45^\circ$) as sketched in Fig. 1(a). Each edge is shared by 3 neighbouring unit cells. Write s_i as the unit tangential vector along a representative cell edge. Now impose a macroscopic strain ε_{ij}^∞ on the Kelvin foam and its

core material. The edge material behaves as a strut of length ℓ and cross-sectional area a . It experiences an axial strain of

$$\varepsilon_a = \varepsilon_{ij}^{\infty} s_i s_j \quad (3.2)$$

and an associated extension

$$e = \varepsilon_a \ell. \quad (3.3)$$

First, treat the cell edges as linear elastic, such that each edge carries an axial tension of

$$T = E_0 a \varepsilon_a, \quad (3.4)$$

Second, treat each cell edges as rigid, ideally plastic in tension but buckles at zero load in compression such that

$$T = \begin{cases} \sigma_0 a & \text{for } \varepsilon_a > 0 \\ 0 & \text{for } \varepsilon_a < 0. \end{cases} \quad (3.5)$$

The macroscopic contribution to modulus ΔE and to uniaxial strength $\Delta \sigma_Y$ due to the affine deformation of the Kelvin foam is determined by stating that the macroscopic stress $\Delta \Sigma_{ij}$ in the foam performs a macroscopic work increment of $V \Delta \Sigma_{ij} \delta \varepsilon_{ij}^{\infty}$ in each Kelvin cell of volume V when the macroscopic virtual strain is $\delta \varepsilon_{ij}^{\infty}$. Then, the macroscopic work increment due to an extension $\delta e^{(I)}$ of each strut I in the volume V is given by

$$V \Delta \Sigma_{ij} \delta \varepsilon_{ij}^{\infty} = \frac{1}{3} \sum_{I=1}^{36} T^{(I)} \delta e^{(I)}. \quad (3.6)$$

where $T^{(I)}$ is the tension in strut I , the summation is taken over all 36 struts (i.e. cell edges) of the unit Kelvin cell and the factor of 1/3 accounts for the fact that each cell edge is shared by 3 neighbouring Kelvin cells.

We proceed to obtain ΔE for uniaxial compression in the x_3 direction. The relative density of the foam is $\bar{\rho} = 4.24(a/\ell^2)$, from (1.4) upon noting that $\omega = 45^\circ$. The volume of unit cell of Kelvin foam has already been given by (1.2). Upon making use of (3.2-3.4), the expression (3.6) can be rephrased as

$$V(\Delta \Sigma_{33} - \Delta \Sigma_{11}) \delta \varepsilon_{33}^{\infty} = \frac{1}{3} \sum_{I=1}^{36} \left[E_0 a \left(\varepsilon_{ij}^{\infty} s_i^{(I)} s_j^{(I)} \right) \ell \left(\delta \varepsilon_{kl}^{\infty} s_k^{(I)} s_l^{(I)} \right) \right]. \quad (3.7)$$

This relation is simplified by noting that $V/(a\ell) = 12/\bar{\rho}$ from (1.4). Now write $\varepsilon_{11}^\infty = \varepsilon_{22}^\infty = -1/2\varepsilon_{33}^\infty$ along with $\delta\varepsilon_{11}^\infty = \delta\varepsilon_{22}^\infty = -(1/2)\delta\varepsilon_{33}^\infty$ to give

$$(\Delta\Sigma_{33} - \Delta\Sigma_{11}) = \frac{\bar{\rho}}{36} E_0 \varepsilon_{33}^\infty \sum_{I=1}^{36} \left(\frac{\varepsilon_{ij}^\infty}{\varepsilon_{33}^\infty} s_i^{(I)} s_j^{(I)} \frac{\delta\varepsilon_{kl}^\infty}{\delta\varepsilon_{33}^\infty} s_k^{(I)} s_l^{(I)} \right). \quad (3.8)$$

The summation is carried out in a routine manner upon writing down the direction cosines $s_i^{(I)}$ of each strut I of the Kelvin unit cell. Numerical evaluation results in

$$(\Delta\Sigma_{33} - \Delta\Sigma_{11}) = \frac{1}{8} \bar{\rho} E_0 \varepsilon_{33}^\infty. \quad (3.9)$$

For the case of uniaxial compression we have $\Delta\Sigma_{11} \equiv 0$ and so

$$\Delta E = \frac{1}{8} \bar{\rho} E_0. \quad (3.10)$$

and so $\alpha_1 = 1/8$.

A similar procedure can be used to determine $\Delta\sigma_Y$, for uniaxial compression with $\varepsilon_{33}^\infty < 0$. Rewrite (3.5) as

$$T^{(I)} = \sigma_0 a \text{H}(-\varepsilon_{ij}^\infty s_i^{(I)} s_j^{(I)}) \quad (3.11)$$

for each strut I , where H is the Heaviside step function. Substitute (3.10) into (3.6) to obtain

$$V(\Delta\Sigma_{33} - \Delta\Sigma_{11})\delta\varepsilon_{33}^\infty = \frac{1}{3} \sum_{I=1}^{36} \left[\sigma_0 a \text{H}(-\varepsilon_{ij}^\infty s_i^{(I)} s_j^{(I)}) \ell \left(\delta\varepsilon_{kl}^\infty s_k^{(I)} s_l^{(I)} \right) \right].$$

which reduces to

$$(\Delta\Sigma_{33} - \Delta\Sigma_{11}) = \frac{\bar{\rho}}{36} \sigma_0 \sum_{I=1}^{36} \left[\text{H}(\varepsilon_{ij}^\infty s_i^{(I)} s_j^{(I)}) \frac{\delta\varepsilon_{kl}^\infty}{\delta\varepsilon_{33}^\infty} s_k^{(I)} s_l^{(I)} \right]. \quad (3.12)$$

Numerical evaluation of the summation term gives

$$\Delta\sigma_Y = \frac{1}{6} \bar{\rho} \sigma_0. \quad (3.13)$$

for the case of uniaxial compression, $\Delta\Sigma_{11} = 0$, and consequently $\alpha_2 = 1/6$.

The affine predictions are approached when the core modulus and core strength are on the order of 0.3 times that of the cell walls, for a relative density in the practical range (of up to 5%), see Fig. 10. It is also noted that there is an intermediate regime that exists when the core has a modulus and strength on the order of 0.03-0.1 times that of the cell walls: for these

values of core properties, the contribution of the cell walls to the macroscopic modulus and strength is approximately mid-way between the affine limit and the empty foam limit.

The main purpose of the present study is to explore the degree to which compressibility of the core affects the macroscopic response. It is shown that the effect is minor as the deformation mode of the closed cell lattice is only changed to a minor degree by imposing a cell-by-cell volumetric constraint. The effect of modulus and strength of core upon the macroscopic response of the composite Kelvin foam and core is explored in Fig. 10. There, it is demonstrated that an incompressible core of sufficiently high modulus and strength changes the deformation mode of the foam from bending to affine-stretching. We anticipate a similar switch in behaviour for the case of a Kelvin foam filled with a compressible core. However, the details would need to be developed in a separate study.

The effect of a finite core modulus and strength upon the macroscopic response of a regular hexagonal honeycomb ($\omega = 30^\circ$) is reported in Appendix B. The findings in Fig. B.1 are qualitatively the same as those given in Fig. 10 for the filled Kelvin foam. For example, when E_c/E_0 and σ_c/σ_0 are sufficiently large the hexagonal honeycomb and core deform in an affine manner. An upper bound for the macroscopic modulus and strength of the filled honeycomb is obtained in a straightforward manner, and analytic predictions can be obtained see (B.1) and (B.2). At the other extreme of very small values of core modulus and strength in relation to that of the cell walls of Kelvin foam, the composite response of the filled regular honeycomb is only slightly above that of the empty regular honeycomb.

4. Concluding discussion

The results of the present study reveal that the effect of an inviscid incompressible core on the compressive response of a 3D closed-cell Kelvin foam is qualitatively different to that of a 2D hexagonal honeycomb. The presence of an incompressible core changes the deformation mode of an elongated hexagonal honeycomb from bending to stretching with subsequent severe softening that results in shear localisation. In contrast, the empty Kelvin foams deform by cell edge bending and cell face stretching, and the imposition of isochoric deformation due to the presence of an inviscid incompressible core has only a small effect upon the macroscopic modulus and yield strength of both the regular and elongated Kelvin cell. However, in the post yield regime, the compressive response is stabilised and no shear bands form when an inviscid incompressible core is present.

The present study gives predictions for the macroscopic response of a closed-cell Kelvin foam that contains a core of finite modulus and strength. Three regimes I to III can be identified in the plots of $\Delta E/E_0$ and $\Delta\sigma_Y/\sigma_0$ of Fig. 10, for a filled Kelvin foam with pronounced Plateau Borders, $\phi = 0.95$. In regime I, the core is sufficiently stiff ($E_c/E_0 > 0.3$) and strong ($\sigma_c/\sigma_0 > 0.3$) for the Kelvin foam to act as a mesh reinforcement and to deform in an affine manner.

The elevation in modulus ΔE and strength $\Delta\sigma_Y$ upon replacing the core by the filled Kelvin foam are given by (3.10) and (3.13) in the affine limit of regime I. Upon restricting attention to $E_c/E_0 > 0.3$ and $\sigma_c/\sigma_0 > 0.3$ the expressions (3.10) and (3.13) satisfy the inequalities

$$\frac{\Delta E}{E_c} < 0.42 \bar{\rho} \text{ and} \quad (4.1)$$

$$\frac{\Delta\sigma_Y}{\sigma_c} < 0.56 \bar{\rho}, \quad (4.2)$$

respectively. Thus, the addition of a Kelvin foam reinforcement to a core, in order to maintain affine deformation of the core, gives only a negligible increase in modulus and strength of the core for the practical case of $\bar{\rho} < 0.05$.

In regime III, the incompressible core is sufficiently compliant ($E_c/E_0 \leq 0.01$) and weak ($\sigma_c/\sigma_0 \leq 0.01$) for the core to give only a slight elevation in modulus and strength of the filled foam above that of the empty foam. The intermediate case is regime II: both the core and Kelvin foam deform in a non-affine manner.

We further note from inspection of Fig. 10 that for $\bar{\rho} = 5\%$, the relative modulus of the filled foam exceeds unity only for a very small value of E_c/E_0 below 0.002. This threshold value of E_c/E_0 decreases with decreasing $\bar{\rho}$. Similarly, $\Delta\sigma_Y/\sigma_0$ exceeds unity only for σ_c/σ_0 less than 0.0045 for $\bar{\rho} = 5\%$, and the threshold value of σ_c/σ_0 drops with decreasing $\bar{\rho}$. Thus, the degree of enhancement of the baseline core properties by the addition of a Kelvin foam is negligible unless the core has a modulus and strength which are more than two orders of magnitude less than those of the cell walls.

Currently, it is a challenge to manufacture 3D closed cell lattices with a filled core. Additive manufacturing methods are evolving that can achieve this. For example, holographic methods will allow such filled foams to be manufactured as they can selectively cure a liquid in 3D and thus cure the walls of a cell with uncured liquid remaining inside it. The present study also serves the role of a basic scoping study to ascertain the degree to which an incompressible core

elevates the macroscopic, effective properties of a closed cell foam. This model problem gives some insight into the mechanical response of biological tissues that contain fluid-filled cells.

Acknowledgements

The authors NF and VSD wish to thank Viggo Tvergaard for many years of technical discussions, and for his international leadership in mechanics. The authors are grateful for financial support from the European Research Council project MULTILAT, grant no. 669764. JC acknowledges support from the Gull & Stellan Ljungberg foundation.

Appendix A: Finite specimen response

All periodic unit cell simulations of filled Kelvin foams display a stable and hardening post-yield stress versus strain response. To search for possible softening modes, which could lead to shear bands forming, finite strain finite element simulations of finite specimens have also been performed. To ensure reasonable run times, ABAQUS/Explicit was used.

A specimen, of height $36\ell \sin \omega$ consisting of $5 \times 5 \times 9$ unit cells, was created by repeating the unit cell, as shown in Fig. A.1(a). The lattice is discretised using shell (S3R) elements, in combination with beam (B31) elements in the case of Plateau Borders. The core is discretised using continuum (C3D4H) elements. The shell and beam elements share nodes with the underlying continuum elements. The element size is chosen as $\ell/5$, which is large enough to allow for a reasonable computation time, but sufficiently small to give accurate values for the stiffness and strength of a periodic unit cell simulation; however, post-yield hardening is slightly over-predicted compared to the finer mesh. This mesh size resulted in a model consisting of 4×10^6 degrees of freedom, for which ABAQUS/Explicit⁴ was employed.

The lattice is assumed to be elastic-perfectly plastic with modulus E_0 , Poisson's ratio $\nu_0 = 0.3$ and yield strength $\sigma_0 = 0.001E_0$. The core has material properties $E_c/E_0 = \sigma_c/\sigma_0 = 0.0003$ and $\nu_c = 0.4999$. The relative density is $\bar{\rho} = 0.03$ when $\omega = 45^\circ$ and $\bar{\rho} = 0.032$ when $\omega = 55^\circ$.

Asymmetric modes of deformation are admitted by the introduction of a suitable edge imperfection. Thus, the core is removed from one cell, as shown in Fig. A1(a). The top and bottom faces are frictionless, and are subjected to compressive velocities $\dot{w}/2$. The boundary velocity \dot{w} is sufficiently small for inertial effects to be negligible. The side faces are traction-free.

Results for finite specimens

Stress versus strain results obtained from simulation of filled finite specimens with $\phi = 0$ and 0.95 are shown in Fig. A.1(b) for $\omega = 45^\circ$ and 55° . The response of the specimens is similar to that of the periodic unit cell with no softening. All specimens deform uniformly without localisation.

⁴ ABAQUS/Explicit version 2020. Dassault Systèmes Simulia Corp., Providence, RI, USA.

Appendix B. Hexagonal honeycomb with an incompressible core of finite modulus and strength

Finite element simulations of the in-plane, plane strain response of a regular hexagonal honeycomb ($\omega = 30^\circ$) was performed using ABAQUS/Standard⁵ in order to determine the sensitivity of the macroscopic modulus and compressive strength to the core properties. The cell walls are meshed with second-order 8-noded plane-strain elements (CPE8 in ABAQUS notation) with a small proportion of six-noded elements (CPE6) to ensure space is filled. The cell wall was discretised into a uniform mesh of element size equal to one third of the bar thickness t , which gave adequate accuracy by a mesh convergence study. The cell walls possess a Young's modulus E_0 , a Poisson ratio of 0.3 and a yield strength $\sigma_0 = 10^{-3}E_0$.

The core was meshed using first order 4-noded reduced integration linear pressure plane strain elements with hourglass control (CPE4RH), and supplemented by a small number of 3-noded plane strain elements (CPE3). The core was discretised into a non-uniform, graded mesh, of size on the order of $t/3$ near the cell walls and $\ell/10$ at the centre of each hexagon. The external nodes of the core elements were tied to the inner nodes of the cell walls, thereby precluding the possibility of separation (cavitation) between core and cell walls. The yield strength σ_c and Young's modulus E_c of the core was varied in proportion such the yield strain of the core equals that of the cell walls, $\varepsilon_0 = \sigma_0/E_0 = 0.001$. The Poisson's ratio of the core material equals 0.4999; consequently, the core is almost incompressible. The periodic unit cell and periodic boundary conditions on the hexagonal honeycomb are the same as those reported in Carlsson et al (2022). The periodic cell calculation delivers the macroscopic nominal stress component σ^∞ which is work-conjugate to the imposed nominal strain ε^∞ in uniaxial compression. The macroscopic Young's modulus of the honeycomb is $E = \sigma^\infty/\varepsilon^\infty = (1 - \bar{\rho})E_c/(1 - \nu^2) + \Delta E$ and macroscopic strength is $\sigma_Y = (1 - \bar{\rho})\sigma_c/\sqrt{1 - \nu + \nu^2} + \Delta\sigma_Y$, where the factor $1/(1 - \nu^2)$ for modulus and $1/\sqrt{1 - \nu + \nu^2}$ for strength arise due to the assumption of plane strain.

⁵ ABAQUS/Standard version 2018. Dassault Systèmes Simulia Corp., Providence, RI, USA.

Results

Plots of $\Delta E/E_0$ and $\Delta\sigma_Y/\sigma_0$ versus $\bar{\rho}$ are given in Fig. B1 for selected values of E_c/E_0 and σ_c/σ_0 . For sufficiently low values of $E_c/E_0 = \sigma_c/\sigma_0 < 0.001$ the core behaves as an almost incompressible solid of negligible shear modulus and the composite response attains a limit curve that is close to the response of the empty, regular hexagonal honeycomb. As E_c/E_0 and σ_c/σ_0 increases, the contribution from the lattice increases. Upper bounds have been obtained in the same manner described in the body of the paper for the Kelvin foam. Upon noting that the hexagonal unit cell has six bars, each shared between two cells, and that the core undergoes deformation such that $\varepsilon_{11}^\infty = -\varepsilon_{22}^\infty$, we obtain as upper bounds the expressions

$$\Delta E = \frac{1}{2}\bar{\rho}E_0 \text{ and} \tag{B.1}$$

$$\Delta\sigma_Y = \frac{1}{3}\bar{\rho}\sigma_0. \tag{B.2}$$

It is noted from Fig. B.1 that the upper bound is approached when the core modulus and strength are on the order of 0.03 to 0.1 times that of the cell walls. We emphasise that the affine calculations have been performed by treating the cell walls as one-dimensional struts that stretch instead of a 2D continuum. There is a much stiffer affine limit of $\Delta E = \bar{\rho}E_0$ and $\Delta\sigma_Y = \bar{\rho}\sigma_0$ that exists for a hexagonal honeycomb when the cell walls are treated as a continuum and the compressive strength of the cell walls is dictated by yield rather than buckling.

References

- Ashby, M.F., Evans, A.G., Fleck, N.A., Gibson, L.J., Hutchinson, J.W. and Wadley, H.N.G., 2000. *Metal Foams: A Design Guide*, June 2000, Butterworth-Heinemann. ISBN 0 7506 7219 6.
- Carlsson, J., Li, K. Deshpande V.S. and Fleck N.A., 2022. The finite strain, elastic-plastic response of a filled hexagonal honeycomb. *J. Mech. Phys. Solids*, **168**, 105047. doi: [10.1016/j.jmps.2022.105047](https://doi.org/10.1016/j.jmps.2022.105047)
- Cartié, D. R. and Fleck, N.A., 2003. The effect of pin reinforcement upon the through-thickness compressive strength of foam-cored sandwich panels. *Compos. Sci. Technol.* **63**(16), 2401-2409.
- Chen, Y., Das, R., Battley, M. and Xu, Z., 2018. Compressive and shear strengths of the ductile closed-cell Kelvin and Weaire-Phelan foams along the lattice direction [100], *Thin-walled structures* **132**, 237-249.
- Comley K and Fleck NA, 2010. A micromechanical model for the Young's modulus of adipose tissue. *Int. J. Solids and Structures* **47**, 2982-2990.
- Deshpande, V.S., Ashby, M. F. and Fleck, N. A., 2001. Foam topology bending versus stretching dominated architectures, *Acta mater.* **49**, 1035-1040.
- Deshpande, V.S. and Fleck, N.A., 2001. Multiaxial yield behaviour of polymer foams, *Acta mater.* **49**, 1859-1866.
- D'Mello, R.J. and Waas, A.M., 2013. Inplane crush response and energy absorption of circular cell honeycomb fill with elastomer. *Compos. Struct.* **106**, 491-501.
- Fleck, N.A., 1997. Compressive failure of fibre composites. *Advances in Applied Mechanics*, Academic Press, **33**, 43-119.
- Gibson, L. J. and Ashby, M. F., 1997. *Cellular solids. Structure and properties – second edition*. Cambridge University Press.
- Han, B, Zhang, Z.J., Zhang, Q.C., Zhang, Q., Lu, T.J. and Lu, B.H., 2017. Recent advances in hybrid-lattice-cored sandwiches for enhanced multifunctional performance. *Extreme Mech. Lett.* **10**, 58-69.

- Jang, W.-Y., Kyriakides, S. and Kraynik, A.M., 2010. On the compressive strength of open-cell metal foams with Kelvin and random cell structures, *Int. J. Solids Structs* **47**, 2872-2883.
- Jang, W.-Y. and Kyriakides, S., 2009. On the crushing of aluminum open-cell foams: Part II analysis, *Int. J. Solids Structs* **46**(2-3), 635-650.
- Lord Kelvin (Sir William Thomson), 1887. On the Division of Space with Minimum Partitional Area, *Philosophical Magazine*, **24**(151): 503, doi:10.1080/14786448708628135.
- Simone, A. E. and Gibson, L. J., 1998. Effects of solid distribution on the stiffness and strength of metallic foams, *Acta mater.* **46**(6), 2139-2150.
- Sullivan, R.M., Ghosn, L.J. and Lerch, B.A., 2008. A general tetrakeidecahedron model for open-cell foams. *Int. J. Solids Structs* **45**(6), 1754-1765.
- Sullivan, R.M., Ghosn, L.J. and Lerch, B.A., 2009. Application of an elongated Kelvin Model to Space Shuttle Foams, *Journal of Spacecraft and Rockets* **46**(2), 411-418.
- Tankasala, H., Deshpande, V.S. and Fleck, N., 2021. The in-plane elastic-plastic response of an incompressible, filled hexagonal honeycomb, *J. Mech. Phys. Solids* **155**, 104536.
- Tvergaard, V., 1982. Material failure by void coalescence in localized shear bands. *Int. J. Solids Structs.*, **18**(8), 659-672.
- Tvergaard, V. and Hutchinson, J.W., 1992. The relation between crack growth resistance and fracture process parameters in elastic-plastic solids. *J. Mech. Phys. Solids* **40**(6), 1377-1397.
- Warren, W. E. and Kraynik, A. M., 1997. Linear elastic behavior of a low-density Kelvin foam with open-cells, *J. Appl. Mech.* **64**, 787-794.
- Weaire, D. and Hutzler, S., 2001. *The physics of foams*. Oxford University Press.
- Weaire, D. and Phelan, R., 1994, A counter-example to Kelvin's conjecture on minimal surfaces, *Phil. Mag. Lett.* **69** (2). 107-110, doi:10.1080/09500839408241577.
- White, B.C., Garland, A., Alberdi, R. and Boyce, B.L., 2021. Interpenetrating lattices with enhanced mechanical functionality. *Addit. Manuf.* **38**, 101741.
- Yan, L.L, Yu, B, Han, B., Chen, C.Q., Zhang, Q.C. and Lu, T.J, 2013. Compressive strength and energy absorption of sandwich panels with aluminium foam-filled corrugated cores. *Compos. Sci. Technol.* **86**, 142-148.

Zhu, H.X., Knott, J.F. and Mills, N.J., 1997a. Analysis of the elastic properties of open-cell foams with tetrakaidecahedral cells. *J. Mech. Phys. Solids* **45** (3), 319-343.

Zhu, H.X., Mills, N.J. and Knott, J.F., 1997b. Analysis of the high-strain compression of open-cell foams. *J. Mech. Phys. Solids* **45** (11-12), 1875-1904.

Figure captions

Fig 1. Hexagonal honeycomb and Kelvin foam. (a) Elongated Kelvin cell, (b) elongated hexagonal honeycomb, (c) volume V of Kelvin cell and hexagon versus angle ω .

Fig. 2. Compressive response of an empty and filled elongated honeycomb of geometry $\omega = 40^\circ$. (a) Nominal stress versus strain response for $\bar{\rho} = 0.08$. The dashed lines are analytical predictions of the initial elastic response, yield and subsequent softening behaviour as given by Tankasala et al. (2021) and Carlsson et al. (2022). (b) Compressive strength σ_Y of empty and filled $\omega = 40^\circ$ honeycomb as a function of relative density $\bar{\rho}$.

Fig. 3. (a) Kelvin polyhedron, (b) periodic, cuboidal unit cell used in finite element simulations (faces omitted), (c) a lattice consisting of 8 open-cell Kelvin polyhedral, indicating the unit cell used in periodic unit cell calculations, (d) cross-section of five faces to show Plateau Borders at their intersections, and (e) finite element representation of Plateau Borders with shell and beam elements.

Fig. 4. Stress versus strain response of periodic unit cell of empty and filled Kelvin foam for the choices $\phi = 0$ and 0.95 . (a) Regular Kelvin foam ($\omega = 45^\circ$) of relative density $\bar{\rho} = 0.03$. (b) Elongated Kelvin foam ($\omega = 55^\circ$) of relative density $\bar{\rho} = 0.032$.

Fig. 5. Empty Kelvin foam with $\phi = 0$ and $\bar{\rho} = 0.03$ in compression at $|\varepsilon^\infty| = 0.006$ (state A) and $|\varepsilon^\infty| = 0.04$ (state B). Contours represent von Mises strain. Deformation is magnified by a factor of x20 in state A and by a factor of x3 in state B.

Fig. 6. Empty Kelvin foam with $\phi = 0.95$ and $\bar{\rho} = 0.03$ in compression at $|\varepsilon^\infty| = 0.006$ (state C) and $|\varepsilon^\infty| = 0.04$ (state D). Contours in the cell faces denote von Mises strain, and contours in the cell edge denote von Mises stress. Deformation is magnified by a factor of x20 in state C and by a factor of x3 in state D.

Fig. 7. Filled Kelvin foam with $\phi = 0$ and $\bar{\rho} = 0.03$ in compression at $|\varepsilon^\infty| = 0.006$ (state E) and $|\varepsilon^\infty| = 0.04$ (state F). Contours represent von Mises strain. Deformation is magnified by a factor of x20 in state E and by a factor of x3 in state F.

Fig. 8. Filled Kelvin foam with $\phi = 0.95$ and $\bar{\rho} = 0.03$ in compression at $|\varepsilon^\infty| = 0.006$ (state G) and $|\varepsilon^\infty| = 0.04$ (state H). Contours in the cell faces denote von Mises strain, and contours in the cell edge denote von Mises stress. Deformation is magnified by a factor of x20 in state G and by a factor of x3 in state H.

Fig. 9. Effect of filling upon the modulus and strength of regular and elongated Kelvin foams. (a) Modulus and (b) strength of regular ($\omega = 45^\circ$) Kelvin foam. (c) Modulus and (d) strength of elongated ($\omega = 55^\circ$) Kelvin foam.

Fig. 10. (a) Modulus and (b) compressive strength of filled Kelvin foam relative to that of the core, for $\omega = 45^\circ$ and $\phi = 0.95$. Regimes I, II and III are identified, as explained in the text. The lower dotted line denotes the response of the empty Kelvin foam.

Fig. A.1. Finite specimen predictions for filled Kelvin foam of $\phi = 0, 0.95$ and $\omega = 45^\circ, 55^\circ$. (a) Finite specimen, consisting of $5 \times 5 \times 9$ unit cells, with an edge defect in the form of a missing cell highlighted in red. (b) Collapse response. The relative density is $\bar{\rho} = 0.03$ for the case of $\omega = 45^\circ$ and $\bar{\rho} = 0.032$ for $\omega = 55^\circ$.

Fig. B.1. Effect of filling of a regular hexagonal honeycomb ($\omega = 30^\circ$) upon (a) macroscopic modulus and (b) macroscopic strength.

Figures

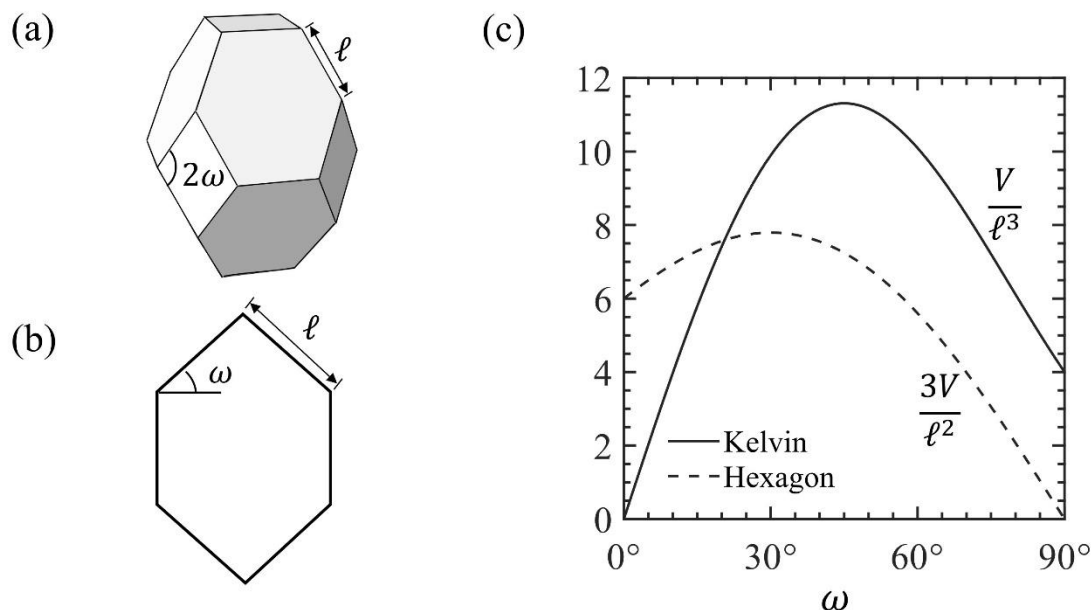


Fig 1. Hexagonal honeycomb and Kelvin foam. (a) Elongated Kelvin cell, (b) elongated hexagonal honeycomb, (c) volume of Kelvin cell and hexagon versus angle ω .

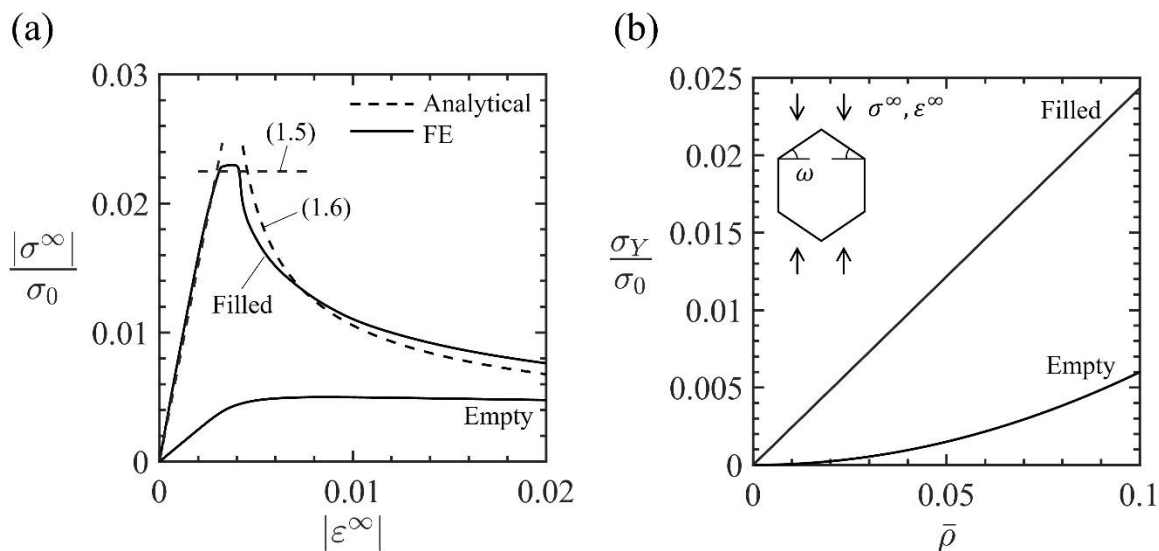


Fig. 2. Compressive response of an empty and filled elongated honeycomb of geometry $\omega = 40^\circ$. (a) Nominal stress versus strain response for $\bar{\rho} = 0.08$. The dashed lines are analytical predictions of the initial elastic response, yield and subsequent softening behaviour as given by Tankasala et al. (2021) and Carlsson et al. (2022). (b) Compressive strength σ_Y of empty and filled $\omega = 40^\circ$ honeycomb as a function of relative density $\bar{\rho}$.

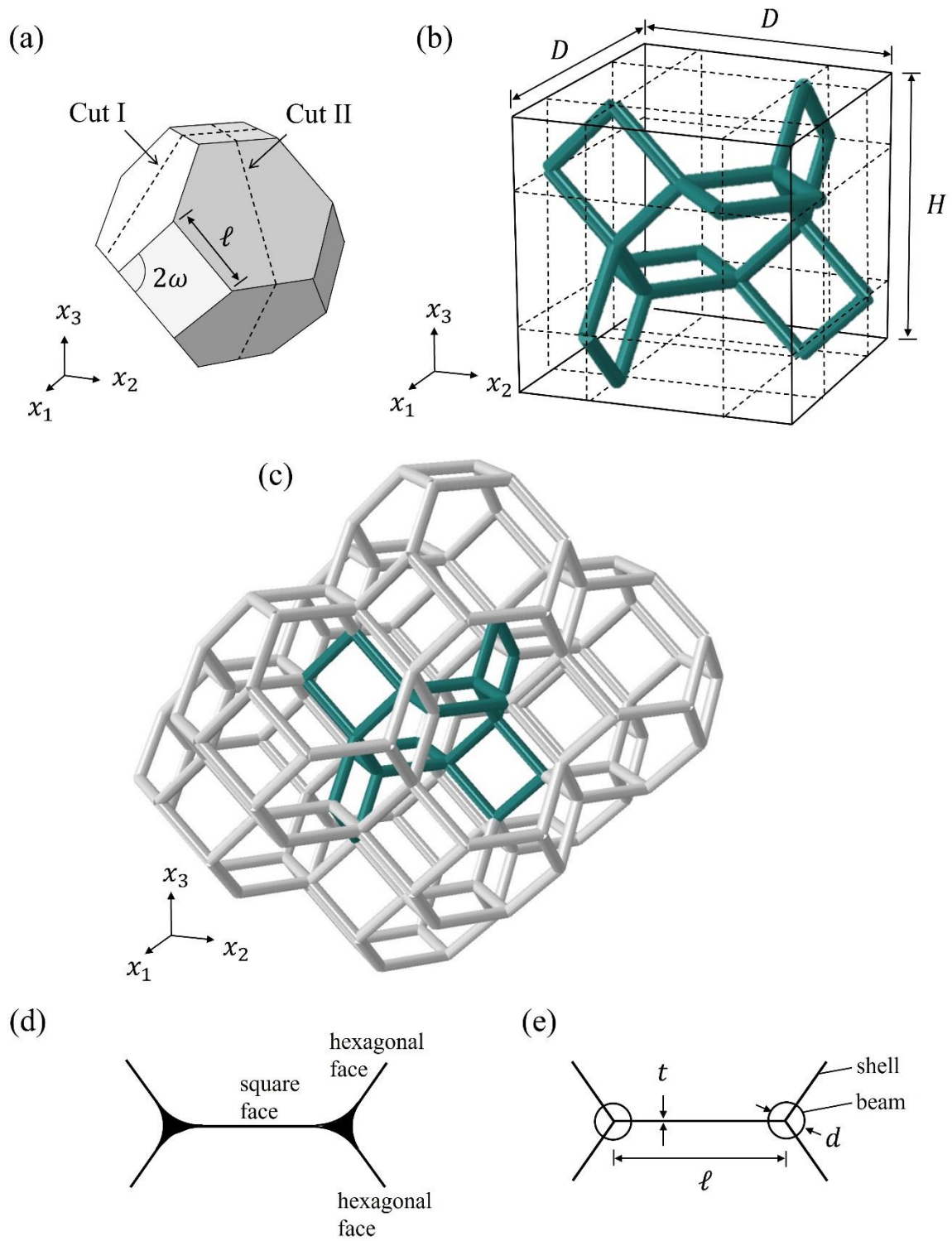


Fig. 3. (a) Kelvin polyhedron, (b) periodic, cuboidal unit cell used in finite element simulations (faces omitted), (c) a lattice consisting of 8 open-cell Kelvin polyhedra, indicating the unit cell used in periodic unit cell calculations, (d) cross-section of five faces to show Plateau Borders at their intersections, and (e) finite element representation of Plateau Borders with shell and beam elements.

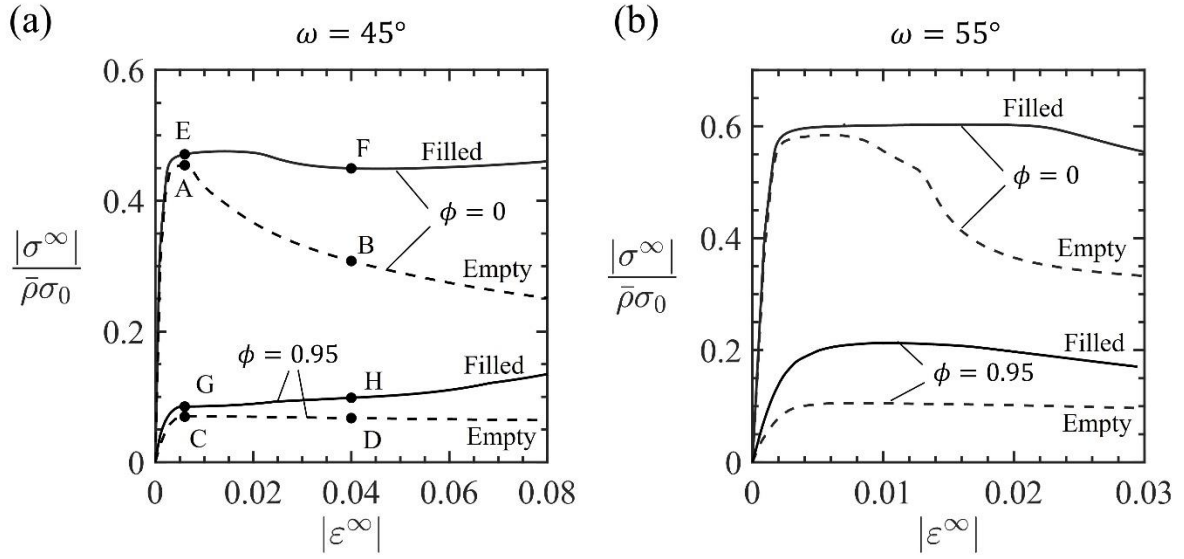


Fig. 4. Stress versus strain response of periodic unit cell of empty and filled Kelvin foam for the choices $\phi = 0$ and 0.95 . (a) Regular Kelvin foam ($\omega = 45^\circ$) of relative density $\bar{\rho} = 0.03$. (b) Elongated Kelvin foam ($\omega = 55^\circ$) of relative density $\bar{\rho} = 0.032$.

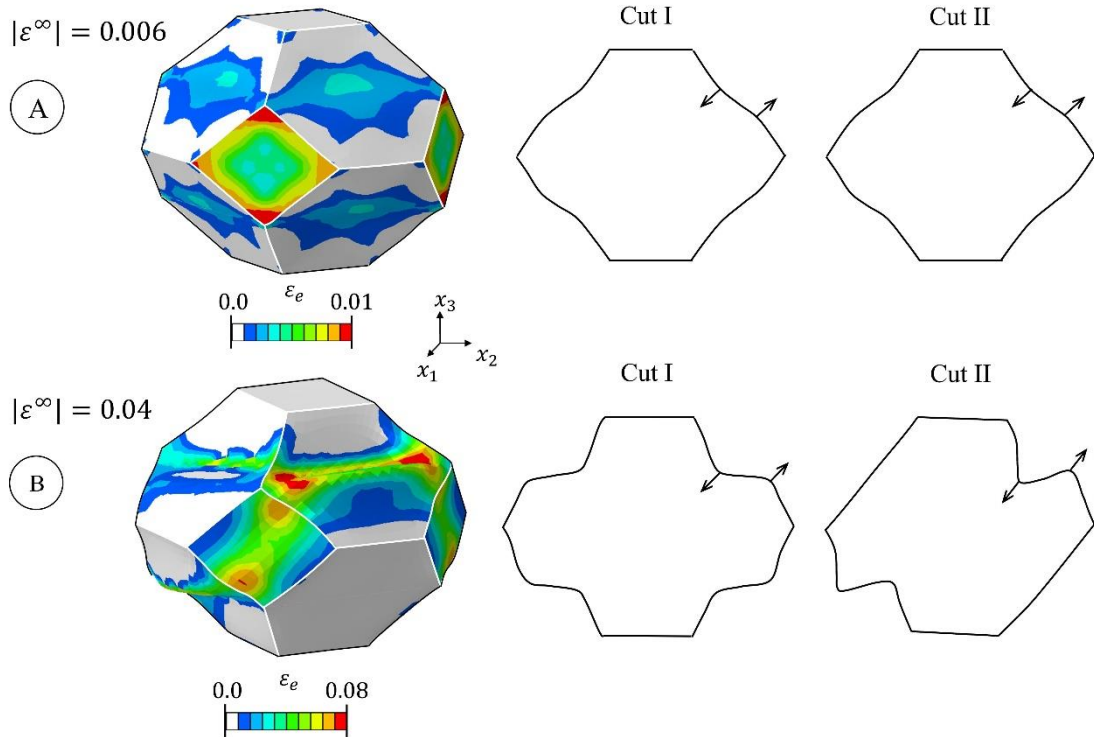


Fig. 5. Empty Kelvin foam with $\phi = 0$ and $\bar{\rho} = 0.03$ in compression at $|\varepsilon^\infty| = 0.006$ (state A) and $|\varepsilon^\infty| = 0.04$ (state B). Contours represent von Mises strain. Deformation is magnified by a factor of $\times 20$ in state A and by a factor of $\times 3$ in state B.

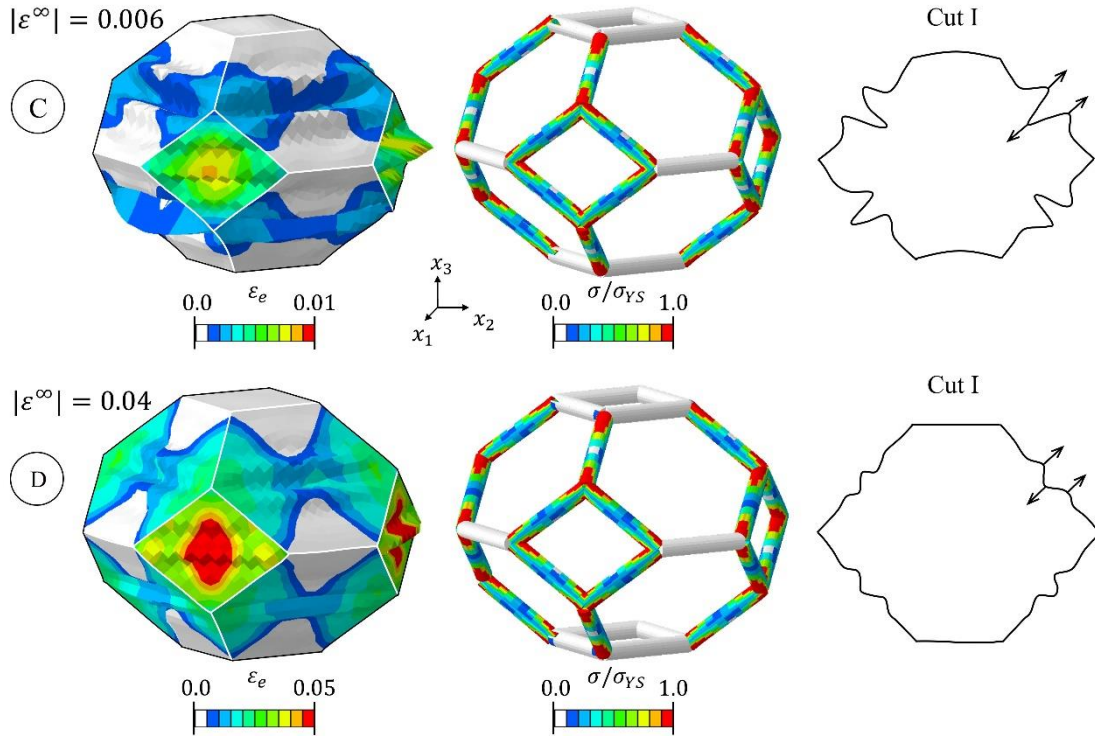


Fig. 6. Empty Kelvin foam with $\phi = 0.95$ and $\bar{\rho} = 0.03$ in compression at $|\varepsilon^\infty| = 0.006$ (state C) and $|\varepsilon^\infty| = 0.04$ (state D). Contours in the cell faces denote von Mises strain, and contours in the cell edge denote von Mises stress. Deformation is magnified by a factor of x20 in state C and by a factor of x3 in state D.

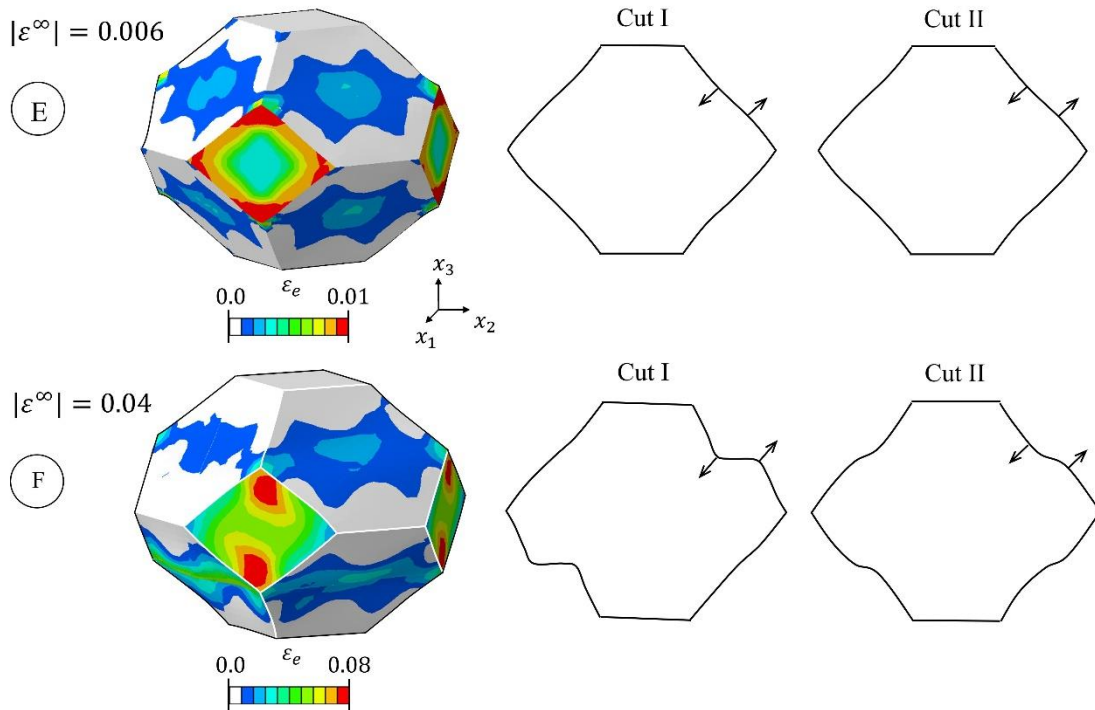


Fig. 7. Filled Kelvin foam with $\phi = 0$ and $\bar{\rho} = 0.03$ in compression at $|\varepsilon^\infty| = 0.006$ (state E) and $|\varepsilon^\infty| = 0.04$ (state F). Contours represent von Mises strain. Deformation is magnified by a factor of x20 in state E and by a factor of x3 in state F.

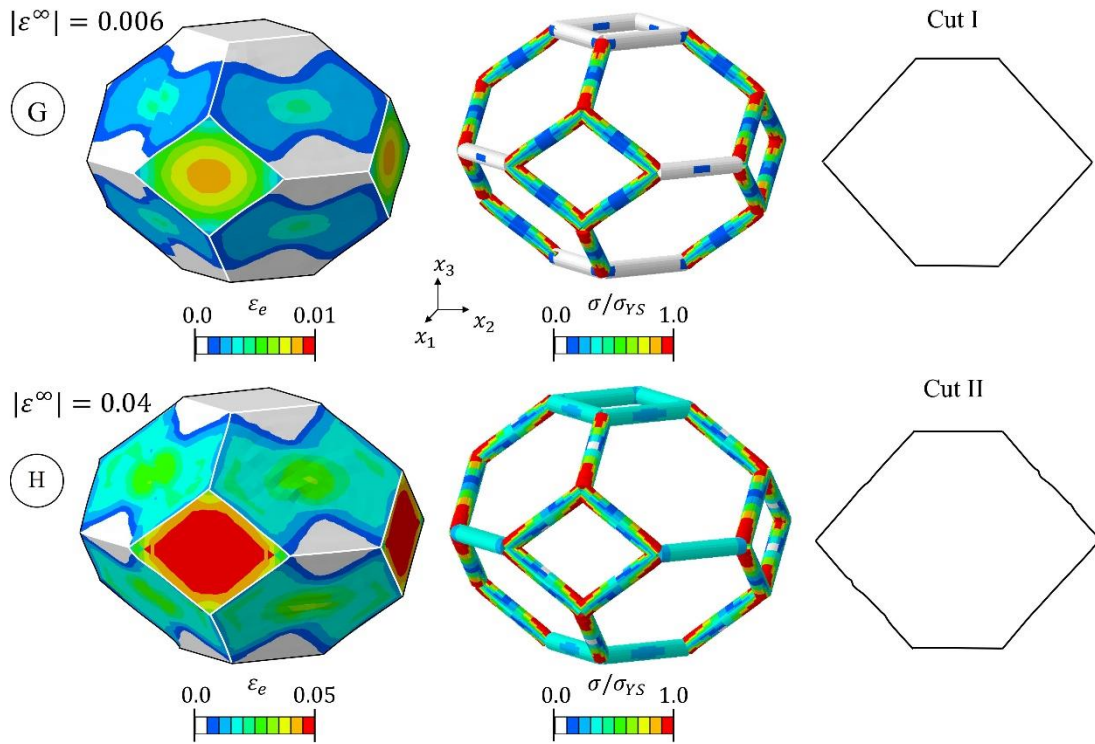


Fig. 8. Filled Kelvin foam with $\phi = 0.95$ and $\bar{\rho} = 0.03$ in compression at $|\varepsilon^\infty| = 0.006$ (state G) and $|\varepsilon^\infty| = 0.04$ (state H). Contours in the cell faces denote von Mises strain, and contours in the cell edge denote von Mises stress. Deformation is magnified by a factor of x20 in state G and by a factor of x3 in state H.

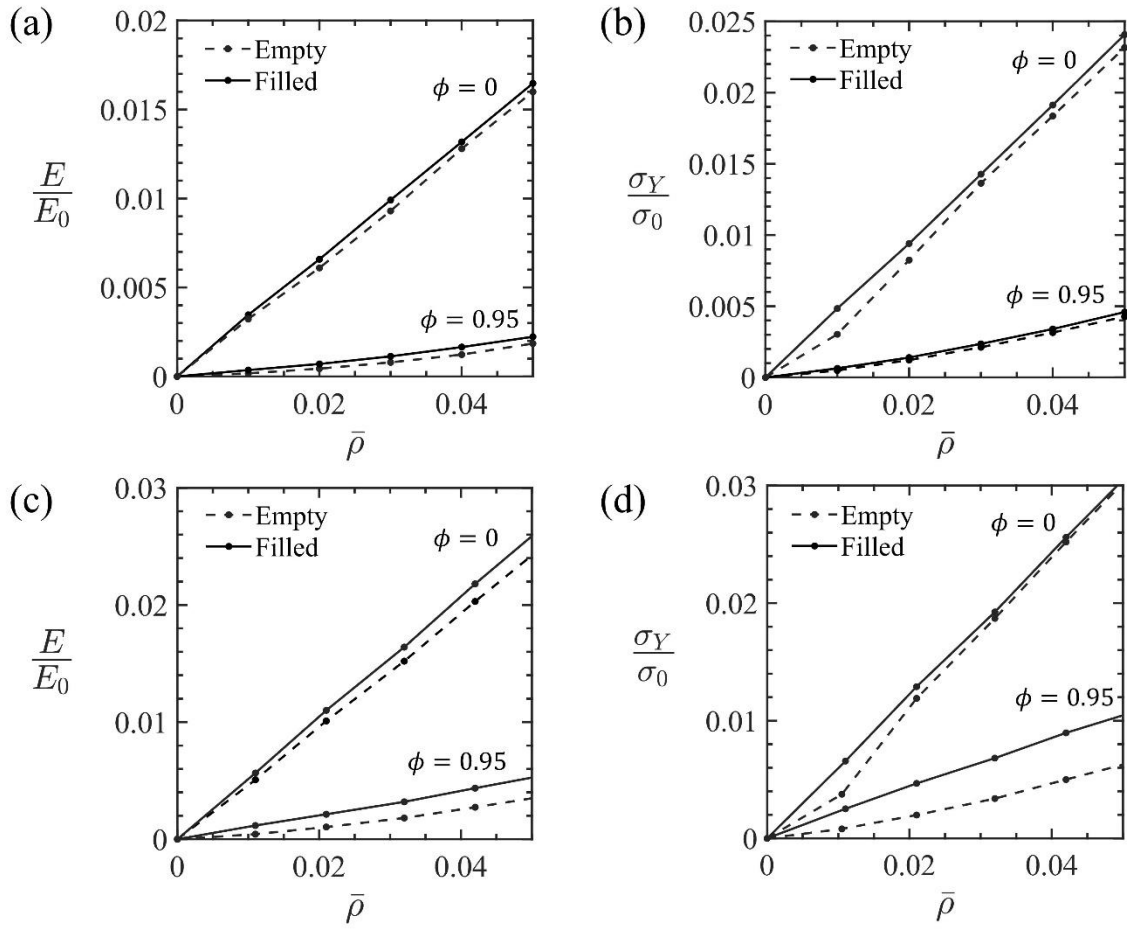


Fig. 9. Effect of filling upon the modulus and strength of regular and elongated Kelvin foams. (a) Modulus and (b) strength of regular ($\omega = 45^\circ$) Kelvin foam. (c) Modulus and (d) strength of elongated ($\omega = 55^\circ$) Kelvin foam.

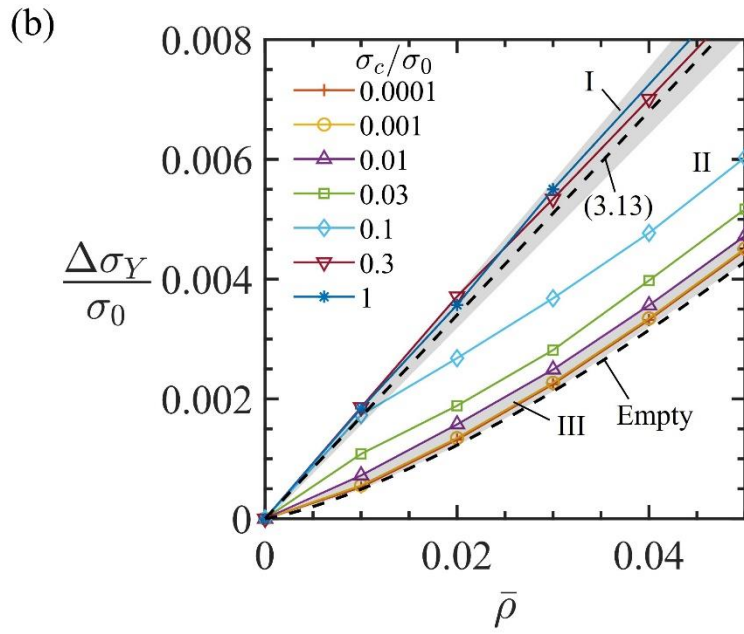
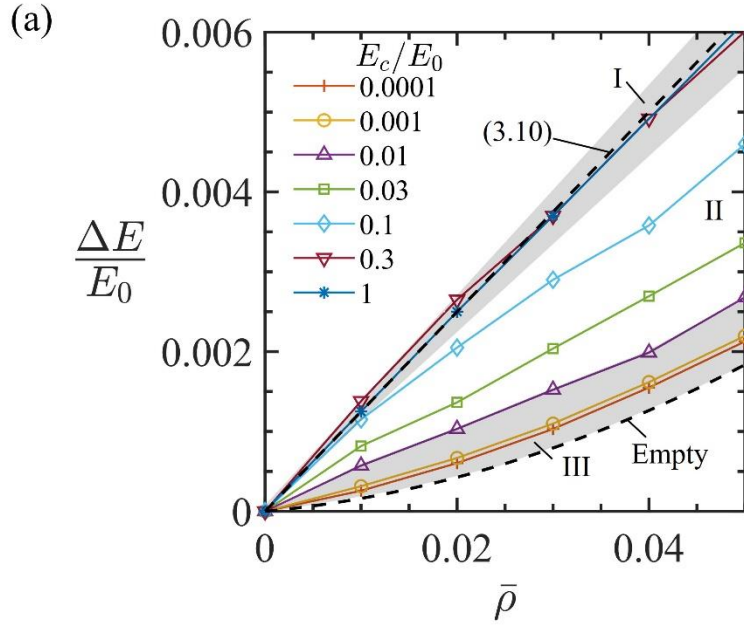


Fig. 10. (a) Modulus and (b) compressive strength of filled Kelvin foam relative to that of the core, for $\omega = 45^\circ$ and $\phi = 0.95$. Regimes I, II and III are identified, as explained in the text. The lower dotted line denotes the response of the empty Kelvin foam.

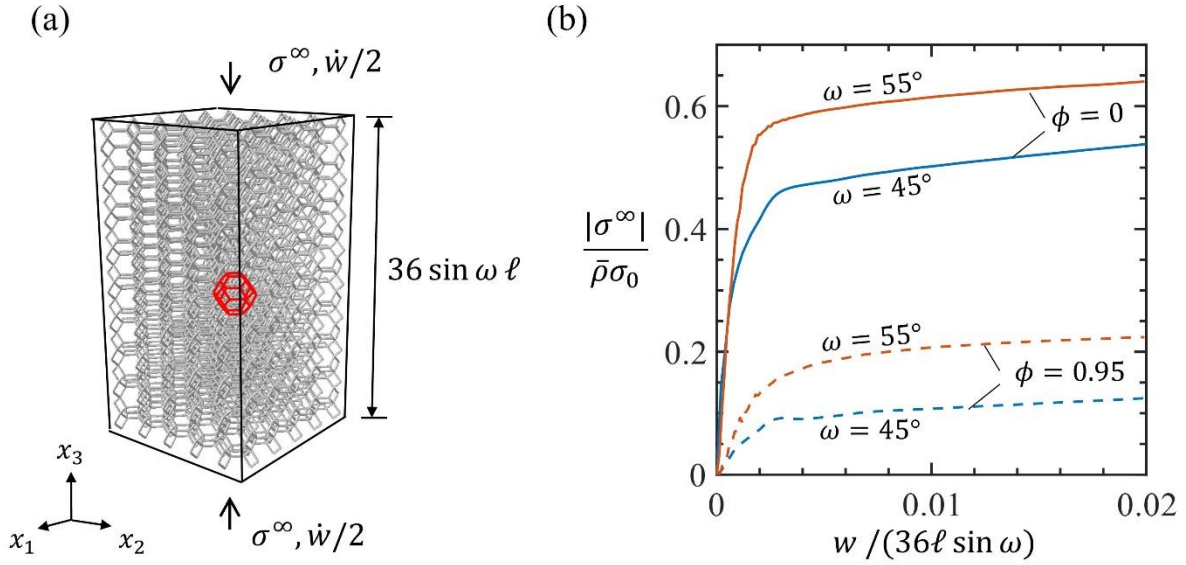


Fig. A.1. Finite specimen predictions for filled Kelvin foam of $\phi = 0, 0.95$ and $\omega = 45^\circ, 55^\circ$. (a) Finite specimen, consisting of $5 \times 5 \times 9$ unit cells, with an edge defect in the form of a missing cell highlighted in red. (b) Collapse response. The relative density is $\bar{\rho} = 0.03$ for the case of $\omega = 45^\circ$ and $\bar{\rho} = 0.032$ for $\omega = 55^\circ$.

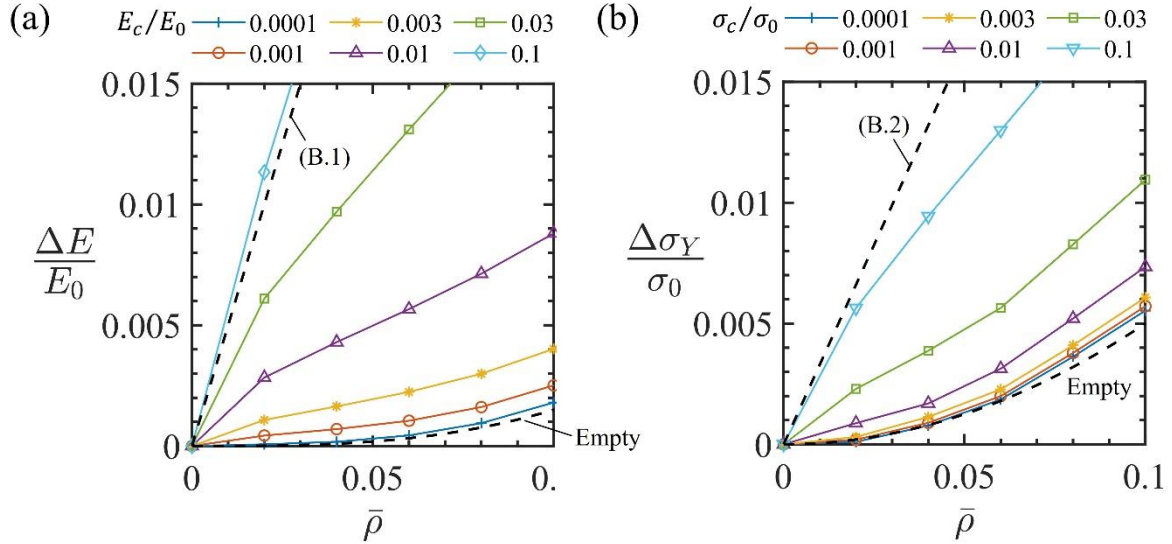


Fig. B.1. Effect of filling of a regular hexagonal honeycomb ($\omega = 30^\circ$) upon (a) macroscopic modulus and (b) macroscopic strength.